

Supplemental Material

S1. Description of GOCART model and emissions used in the present study

Details of the GOCART model are described in our previous publications (e.g., Chin et al., 2000, 2002, 2007, 2009; Ginoux et al., 2001, 2004). For the present work, the meteorological fields from the Modern-Era Retrospective Analysis for Research and Applications (MERRA) (Rienecker et al., 2011), produced with version 5 of the Goddard Earth Observing System Data Assimilation System (GEOS5-DAS), are used with a GOCART configuration at a horizontal resolution of 2.5° longitude by 2° latitude and 72 vertical levels from the surface to 0.01 hPa. Aerosol simulations in GOCART include the major aerosol types of sulfate, dust, black carbon (BC), organic matter (OM) (or organic carbon OC, typically $OM = OC \cdot f$ where $f=1.4$ to 2.2 in the literature, and we use 1.4 here), and sea-salt, and the precursor gas species of SO_2 and dimethyl sulfide (DMS). It also contains another natural aerosols specie, methanesulfonate (MSA, also known as methanesulfonic acid), which is formed from a branch of DMS atmospheric oxidation. The model accounts for emissions from fossil fuel and biofuel combustion, biomass burning, volcanic eruptions, vegetation, deserts, and oceans, and simulates atmospheric processing of aerosols including chemistry, convection, advection, boundary layer mixing, dry and wet deposition, and gravitational settling. The model uses the prescribed oxidant fields of OH, H_2O_2 , and NO_3 for sulfur chemistry that are produced from Goddard Chemistry Climate Model (CCM) (Oman et al., 2011) simulations conducted as part of the Atmospheric Chemistry and Climate Model Intercomparison Project (ACCMIP) project (Lamarque et al., 2013). Aerosol particle sizes from 0.01 to 10 μm are included with parameterized hygroscopic growth, which depends on the ambient relative humidity (RH) and aerosol type. Aerosol extinction is calculated as the product of dry aerosol mass and the mass extinction efficiency of each species; the latter is calculated as a function of particle refractive index, size distribution, density, and ambient RH. A recent update includes dust optical properties that are calculated with the T-matrix code (Dubovik et al., 2006) to account for the non-spherical shape of dust particles (Mishchenko et al., 1997). With the same dust refractive indices (Hess et al., 1998), the T-Matrix calculation of spheroid dust particle shape has shown an increase of dust scattering efficiency by up to 10% at 550 nm, and a much stronger decrease of back scattering efficiency by a factor of about 2.5 compared to Mie calculations for spherical particles (Chin et al., 2002, 2009; Yu et al., 2010).

Emissions of SO₂, BC, and OC from fossil fuel and biofuel combustions and biomass burning are taken from the emission dataset A2-ACCMIP (Diehl et al., 2012), which is one of the multi-year emission datasets available from the international initiative AeroCom project (<http://aerocom.met.no>) for its second phase (A2) hindcast model experiments. Fossil fuel/biofuel combustion emissions in A2-ACCMIP are from a combination of the historic emissions developed for ACCMIP (Lamarque et al., 2010) for the time period of 1980-2000 and the emission projection from the Representative Concentration Pathways Scenario 8.5 (RCP8.5) (Riahi et al., 2011) after 2000. Annual anthropogenic emissions are generated by linear interpolation of the original ACCMIP and RCP8.5 emissions that were given in decadal increments (plus year 2005 in RCP8.5) (Diehl et al., 2012). The A2-ACCMIP biomass burning emissions from 1980 to 2008 are presented in Granier et al. (2011) as a part of the MACCity (Monitoring Atmospheric Composition & Climate/Megacity-Zoom for the Environment) project. They were generated by integrating the monthly emissions from the Reanalysis of the Tropospheric Chemical Composition (RETRO, Schultz et al., 2008) between 1980 and 1996 and the Global Fire Emission Dataset Version 2 (GFED v2) (van der Werf et al., 2006) between 1997 and 2008. Biomass burning emission after 2008 is from a linear interpolation of the RCP8.5 dataset (details of A2-ACCMIP dataset can be found in Diehl et al., 2012 and references therein). Unlike our previous simulations of biomass burning emissions when we applied vegetation type-independent emission factors to dry mass burned to estimate tracer emissions from biomass burning (e.g., Chin et al., 2009), here we use the species emissions provided by A2-ACCMIP based on the emission factors from Andreae and Merlet (2001) and updates (Lamarque et al., 2010).

Volcanic SO₂ emissions are taken from a recently compiled database that includes emission amounts and plume heights (Diehl et al., 2012). The database considers 1167 active volcanoes during 1979-2009 based on the volcanic activity database from the Smithsonian Institution's Global Volcanism Program (<http://www.volcano.si.edu/>), the satellite observations of SO₂ from the Total Ozone Mapping Spectrometer (TOMS) and the Ozone Monitoring Instrument (OMI), and ancillary information from other observations reported in the literature. Global volcanic SO₂ emissions are first calculated based on empirical relationships between the Volcanic Explosivity Index (VEI), the Volcanic Sulfur Index (VSI) and the emission amount (Schnetzler et al., 1997; Chin et al., 2000); such estimates are replaced with available TOMS or OMI observations.

Emissions from quasi-continuously erupting (Andres and Kasgnoc, 1998) and silently degassing volcanoes (Berresheim and Jaeschke, 1983; Stoiber et al., 1987) are also included.

Dust emissions are calculated as a function of surface topography, surface bareness, 10-m wind speed, and ground wetness (Ginoux et al., 2001) as follows:

$$E = C S s(r) u_{10m}^2 (u_{10m} - u_t) \quad (1)$$

where E is the dust emission flux, C is a dimensional constant, S is the dust source function (or erodibility) which is a product of the fraction of surface bareness and the topographic depression, $s(r)$ is the fraction of each size class of effective radius r emitted, u_{10m} is the 10-m wind velocity, and u_t is the threshold wind velocity which is determined by the particle size and density and ground wetness w . The w also serves as a switch such that dust will only be mobilized when w from the meteorological field (MERRA in this study) is below a threshold value (i.e., the ground is dry enough, currently w is set to 0.35 in the current version). Recently we have incorporated a newly developed dynamic S into the model (Kim et al., 2013). Instead of using the “static” surface bareness from the land cover classification dataset as in previous GOCART simulations, we determine the surface bareness with the 8-km Normalized Difference Vegetation Index (NDVI) data from AVHRR at twice-per-month time resolution (Tucker et al., 2005; Brown et al., 2006) from 1981 to present. NDVI is usually very low when the ground is bare and increases as ground is covered by more vegetation. We choose a threshold NDVI value of 0.15, below which the surface is considered to be bare. The percentage bareness in each model grid cell is determined by the ratio of the number of bare pixels to the total number of 8-km NDVI pixels within the grid cell. This dynamic dust source function considers the seasonal and interannual variations of the surface bareness, which is shown to improve simulated temporal variation of dust aerosols over some semi-arid areas (details in Kim et al., 2013).

Other emissions include oceanic production of sea salt aerosol and DMS and terrestrial biogenic sources of OC that are converted from monoterpene emission. These sources are the same as described in our previous publications (Chin et al., 2002, 2009, and the references therein) with an update of monthly DMS seawater concentrations from a more recent study (Lana et al., 2011). Note that both DMS seawater concentrations and monoterpene emissions are used as “climatology”, i.e., inter-annual variability is not considered, even though they provide monthly variations of spatial distributions and intensity.

The GOCART model has been evaluated extensively against the remote sensing and in-situ data, as shown in our previous publications. The degree of agreement depends on the model physical/chemical/optical parameters, the input meteorological fields, and the input emission datasets. The overall statistics of the comparisons of GOCART with monthly AOD or concentration data from all AERONET, IMPROVE, EMEP, and University of Miami sites (regardless of measurement duration) are listed in Table S1 below.

Table S1. Statistics* of model comparisons with ground-based observations of monthly averaged quantities.

Network	Quantity	<i>R</i>	<i>E</i>	<i>B</i>	<i>S</i>
AERONET	AOD				
<i>Land source regions:</i>					
	USA	0.571	0.007	1.040	0.612
	EUR	0.387	0.082	1.014	0.691
	EAS	0.691	0.210	0.773	0.536
	SAS	0.707	0.253	0.591	0.759
	SAM	0.720	0.186	0.485	0.421
	SEA	0.712	0.240	0.455	0.508
	SHR	0.822	0.092	1.215	0.838
	SHL	0.612	0.216	1.268	0.731
	MDE	0.756	0.165	1.355	0.748
	CAS	0.578	0.084	1.183	0.766
<i>Ocean regions:</i>					
	NAT	0.546	0.090	1.189	0.514
	CAT	0.849	0.099	1.030	0.904
	SAT	0.511	0.105	0.419	0.514
	WNP	0.619	0.094	1.016	0.809
	NIN	0.750	0.218	1.146	0.402
	SOU	0.450	0.035	1.414	0.605
IMPROVE (U.S.)	Sulfate	0.834	1.065	1.315	0.877
	BC	0.529	0.243	0.631	0.682
	OC	0.466	1.266	0.564	0.575
	Fine dust	0.586	0.952	1.584	0.772
EMEP (Europe)	SO ₂	0.654	4.917	1.892	0.774
	Sulfate	0.534	0.999	1.223	0.752
Arctic	Sulfate	0.743	0.672	1.295	0.870
Univ. Miami (islands)	Sulfate	0.798	0.461	1.043	0.897
	MSA	0.522	0.019	0.539	0.739
	Dust	0.739	21.41	1.974	0.643
	Sea salt	0.410	11.43	1.272	0.664

* The statistic quantities include the correlation coefficient *R*, the root-mean-square-error *E*, the mean bias *B* (defined as the ratio of the model results to the data), and the skill score *S* (a combined measure of correlation and standard error between observation and model, see Taylor, 2001).

S2. Data quality

In this work, we use data from three sources: satellites, AERONET and ground-based in situ sampling. The satellite products have been extensively validated in the past, with known

uncertainties published in the literature. For example, the published accuracy for the satellite data are: MODIS AOD $0.03 \pm 5\%$ over ocean and $0.05 \pm 15\%$ over land (Remer et al., 2008; Levy et al., 2010), MISR AOD 0.05 or 20% (whichever is larger) globally and better over ocean (Kahn et al., 2010), SeaWiFS AOD $0.03 \pm 15\%$ over ocean and $0.05 \pm 20\%$ over land (Sayer et al., 2012a, b), and TOMS AOD $>30\%$ (Torres et al., 2002, 2005). For AERONET the accuracy of AOD is 0.01-0.02 (Eck et al., 1999). The IMPROVE network reported the data accuracies are 4% for sulfate, 15% for OC, 29% for BC, and $>20\%$ for soil dust (IMPROVE data guide, U.C. Davis, 1995). The University of Miami data uncertainties are estimated at $\pm 7\%$ for sulfate, MSA, and Cl^- and $\pm 5\%$ for Na^+ . The none-seasalt-sulfate is then calculated as $[\text{total sulfate} - 0.2517 \times \text{Na}^+]$ to take into account for the sulfate/ Na^+ mass ratio of 0.2517 in bulk seawater (Savoie et al., 1989). Dust concentration is calculated from the measured aluminum concentrations and the average percentage of aluminum in the mineral dust (Arimoto et al., 1995). The data accuracy from EMEP varies among sites and nation. For example, the reported data precision or uncertainty is in the range from a few percent to over 10% for SO_2 and sulfate for the EMEP data quality in 2005 (Aas, 2007).

Since our study is focused on the 30-year trends, the degree of data accuracy is not expected to impact our analysis of the trends or interannual variabilities, as far as the instrument does not systematically drift over the measurement period.

References

- Aas, W., Data quality 2005, quality assurance, and field comparisons, EMEP/CCC-Report 3/2007, 2007 (<http://www.nilu.no/projects/ccc/reports/cccr3-2008.pdf>).
- Andreae, M. O., and Merlet, P.: Emission of trace gases and aerosols from biomass burning, *Global Biogeochem. Cycles*, 15, 955-966, 2001.
- Andres, R. J., and Kasgnoc, A. D.: A time-averaged inventory of subaerial volcanic sulfur emissions, *J. Geophys. Res.*, 103, 25,251-25,261, 1998.
- Arimoto, R., Duce, R. A., Ray, B. J., Ellis Jr, W. G., Cullen, J. D., and Merrill, J. T.: Trace elements in the atmosphere over the North Atlantic, *Journal of Geophysical Research*, 100, 1199-1213, 1995.
- Berresheim, H., and Jaeschke, W.: The Contribution of volcanoes to the global atmospheric sulfur budget, *J. Geophys. Res.*, 88, 3732-3740, 1983.
- Brown, M. E., Pinzon, J. E., Didan, K., Morisette, J. T., and Tucker, C. J.: Evaluation of the consistency of long-term NDVI time series derived from AVHRR, SPOT-Vegetation, SeaWiFS, MODIS and LandsAT ETM+, *IEEE Trans. Geosci. Rem. Sens.*, 44, 1787-1793, 2006.

- Chin, M., Rood, R. B., Lin, S.-J., Müller, J.-F., and Thompson, A. M.: Atmospheric sulfur cycle in the global model GOCART: Model description and global properties, *J. Geophys. Res.*, 105, 24,661-24,687, 2000.
- Chin, M., Ginoux, P., Kinne, S., Torres, O., Holben, B. N., Duncan, B. N., Martin, R. V., Logan, J. A., Higurashi, A., and Nakajima, T.: Tropospheric aerosol optical thickness from the GOCART model and comparisons with satellite and sunphotometer measurements, *J. Atmos. Sci.*, 59, 461-483, 2002.
- Chin, M., Diehl, T., Ginoux, P., and Malm, W.: Intercontinental transport of pollution and dust aerosols: implications for regional air quality, *Atmos. Chem. Phys.*, 7, 5501–5517, 2007.
- Chin, M., Diehl, T., Dubovik, O., Eck, T. F., Holben, B. N., Sinyuk, A., and Streets, D. G.: Light absorption by pollution, dust and biomass burning aerosols: A global model study and evaluation with AERONET data, *Ann. Geophys.*, 27, 3439-3464, 2009.
- Diehl, T., Heil, A., Chin, M., Pan, X., Streets, D., Schultz, M., and Kinne, S.: Anthropogenic, biomass burning, and volcanic emissions of black carbon, organic carbon, and SO₂ from 1980 to 2010 for hindcast model experiments, *Atmos. Chem. Phys. Discuss.*, 12, 24895–24954, 2012.
- Dubovik, O., Sinyuk, A., Lapyonok, T., Holben, B. N., Mishchenko, M., Yang, P., Eck, T. F., Volten, H., Muñoz, O., Veihelmann, B., van der Zande, W. J., Leon, J.-F., Sorokin, M., and Slutsker, I.: Application of spheroid models to account for aerosol particle nonsphericity in remote sensing of desert dust, *J. Geophys. Res.*, 111, D11208, doi:10.1029/2005JD006619, 2006.
- Ginoux, P., Chin, M., Tegen, I., Prospero, J., Holben, B., Dubovik, O., and Lin, S.-J.: Sources and global distributions of dust aerosols simulated with the GOCART model, *J. Geophys. Res.* 106, 20,255-20,273, 2001.
- Ginoux, P., Prospero, J., Torres, O., and Chin, M.: Long-term simulation of dust distribution with the GOCART model: Correlation with the North Atlantic Oscillation, *Environ. Modeling and Software*, 19, 113-128, 2004.
- Granier, C., Bessagnet, B., Bond, T., et al.: Evolution of anthropogenic and biomass burning emissions of air pollutants at global and regional scales during the 1980–2010 period, *Climatic Change*, 109, 163–190, doi:10.1007/s10584-011-11 0154-1, 2011.
- Hess, M., Koepke, P., and Schult, I.: Optical Properties of Aerosols and Clouds: The software package OPAC, *Bull. Amer. Met. Society*, 79, 831-844, 1998.
- Kahn, R. A., Gaitley, B. J., Garay, M. J., Diner, D. J., Eck, T., Smirnov, A., and Holben, B. N.: Multiangle Imaging SpectroRadiometer global aerosol product assessment by comparison with the Aerosol Robotic Network. *J. Geophys. Res.* 115, D23209, doi: 10.1029/2010JD014601, 2010.
- Kim, D., Chin, M., Bian, H., Tan, Q., Brown, M. E., Zheng, T., You, R., Diehl, T., Ginoux, P., and Kucsera, T.: The effect of the dynamic surface bareness on dust source function, emission, and distribution, *J. Geophys. Res.*, 118, 1-16, doi:10.1029/2012JD017907, 2013.
- Lamarque, J. F., et al., The Atmospheric Chemistry and Climate Model Intercomparison Project (ACCMIP): overview and description of models, simulations, and climate diagnostics, *Geosci. Model Dev.*, 6, 179-206, 2013.
- Lana, A., Bell, T. G., Simo, R., et al., An updated climatology of surface dimethylsulfide concentrations and emission fluxes in the global ocean, *Global Biogeochem. Cycles*, 25, GB1004, doi:10.1029/2010GB003850, 2011.

- Levy, R. C., Remer, L. A., Kleidman, R. G., Mattoo, S., Ichoku, C., Kahn, R., and Eck, T. F.: Global evaluation of the Collection 5 MODIS dark-target aerosol products over land, *Atmos. Chem. Phys.*, 10, 10399–10420, 2010.
- Mishchenko, M. I., Travis, L. D., Kahn, R. A., and West, R. A.: Modeling phase functions for dustlike tropospheric aerosols using a shape mixture of randomly oriented polydisperse spheroids, *J. Geophys. Res.*, 102, 16831–16847, doi:10.1029/96JD02110, 1997.
- Oman, L. D., Ziemke, J. R., Douglass, A. R., Waugh, D. W., Lang, C., Rodriguez, J. M., and Nielsen, J. E.: The response of tropical tropospheric ozone to ENSO, *Geophys. Res. Lett.*, 38, L13706, doi:10.1029/2011GL047865, 2011.
- Remer, L., Kleidman, R., Levy, R., Kaufman, Y., Tanre, D., Mattoo, S., et al.: Global aerosol climatology from the MODIS satellite sensors, *J. Geophys. Res.-Atmos.*, 113(D14), D14S07, doi:10.1029/2007JD009661, 2008.
- Savoie, D. L., Prospero, J. M., and Saltzman, E. S.: Non-sea-salt sulfate and nitrate in trade wind aerosols at Barbados: evidence for long-range transport, *J. Geophys. Res.*, 94, 5069-5080, 1989.
- Sayer, A. M., Hsu, N. C., Bettenhausen, C., Ahmad, Z., Holben, B. N., Smirnov, A., Thomas, G. E., and Zhang, J.: SeaWiFS Ocean Aerosol Retrieval (SOAR): Algorithm, validation, and comparison with other data sets, *J. Geophys. Res.*, 117, D03206, doi:10.1029/2011JD016599, 2012a.
- Sayer, A. M., Hsu, N. C., Bettenhausen, C., Jeong, M.-J., Holben, B. N., and Zhang, J.: Global and regional evaluation of over-land spectral aerosol optical depth retrievals from SeaWiFS, *Atmos. Meas. Tech.*, 5, 1761-1778, doi:10.5194/amt-5-1761-2012, 2012b.
- Schnetzler, C. C., Bluth, G. J. S., Krueger, A. J., and Walter, L. S.: A proposed volcanic sulfur dioxide index (VSI), *J. Geophys. Res.*, 102, 20,087-20,091, 1997.
- Schultz, M. G., Heil, A., Hoelzemann, J. J., Spessa, A., Thonicke, K., Goldammer, J., Held, A. C., Pereira, J. M., and van het Bolscher, M.: Global Wildland Fire Emissions from 1960 to 2000, *Global Biogeochem. Cyc.*, 22, GB2002, doi:10.1029/2007GB003031, 2008.
- Stoiber, R. E., Williams, S. N., and Huebert, B.: Annual contribution of sulfur dioxide to the atmosphere by volcanoes, *J. Volcanol. Geotherm. Res.*, 33, 1-8, 1987.
- Taylor, K. E., Summarizing multiple aspects of model performance in a single diagram, *J. Geophys. Res.*, 106, 7183-7192, 2001.
- Tucker, C. Pinzon, J., J. E., Brown, M. E., Slayback, D., Pak, E. W., Mahoney, R., Vermote, E., and El Saleous, N.: An extended AVHRR 8-km NDVI data set compatible with MODIS and SPOT vegetation NDVI data, *Int. J. Remote Sens.*, 26, 4485–4498, 2005.
- van der Werf, G. R., Randerson, J. T., Giglio, L., Collatz, G. J., Kasibhatla, P. S., and Arellano, A. F., Jr.: Interannual variability in global biomass burning emissions from 1997 to 2004, *Atmos. Chem. Phys.*, 6, 3423–3441, 2006.
- Yu, H., Chin, M., Winker, D. M., Omar, A. H., Liu, Z., Kittaka, C., and Diehl, T.: Global view of aerosol vertical distributions from CALIPSO lidar measurements and GOCART simulations: Regional and seasonal variations. *J. Geophys. Res.*, 115, D00H30, doi:10.1029/2009JD013364, 2010.

Fig. S1. Global sources of fossil fuel/biofuel (FF) OC+BC (top left), biomass burning (BB) OC+BC (top right), FF+BB SO₂+sulfate (2nd row left), DMS (2nd row right), volcanic SO₂ (3rd row left), biogenic OC (3rd row right), dust (bottom left), and sea salt (bottom right) in 2001. The latter five are considered as natural sources.

Fig. S2. Number of satellite data points of annual average AOD in 2001 for deriving the “data diversity” shown in Fig. 5 in the main section.

Fig. S3a. Regional annual average AOD from 1980 to 2009 for all 15 land regions. Region domains are shown in Fig. 1 and names listed in Table 1 in the main section. Legends are the same as Fig. 6a in the main section.

Fig. S3b. Regional annual average AOD from 1980 to 2009 for all 12 ocean regions. Region domains are shown in Fig. 1 and names listed in Table 1 in the main section. Legends are the same as Fig. 6b in the main section.

Fig. S4. Left column: Monthly AOD from AERONET and GOCART at seven sites that have data for at least 12 years but are not shown in Fig. 7 in the main section (site locations are shown in small circles in Fig. 3a). Right column: Ratio of annual mean AOD to the 2000-2001 average at corresponding sites. Legends are the same as Fig. 7. (Note: results over Mauna Loa are not shown because the AERONET sites is at 3.5 km but the model and satellite AOD contain significant amount PBL aerosols at their 2.5°×2° and 1°×1° spatial resolution, so the results are not comparable; and results over Wallops Island are also not shown because they are similar to GSFC for their close locations.)

Fig. S5. Changes of surface concentration of sulfate expressed as the ratio of annual average to the 2000-2001 average for (left) IMPROVE and (right) EMEP measurements at sites with at least 15 years of data from the 1980s to 2000s. Data are shown in light blue and model results in dark grey.

Fig. S6. Monthly surface concentrations (left column) and trends (right column) of sulfate and sea salt at American Samoa (top two panels) and sulfate and MSA at Mauna Loa Observatory. Data at American Samoa are from University of Miami, and that at Mauna Loa are from University of Hawaii. Site locations are in Fig. 3b (small red and orange circles, respectively, for Samoa and MLO). Legends are the same as Fig. 8.

Fig. S7. Explanation of the criteria used for the election of the two time segments used in section 4.4 and Fig. 11a and Fig. 11b in the main section. Criteria include: (1) excluding the years with large volcanic influences (not shown), (2) choosing the time with maximum satellite data sets, and (3) avoiding extreme ENSO years.

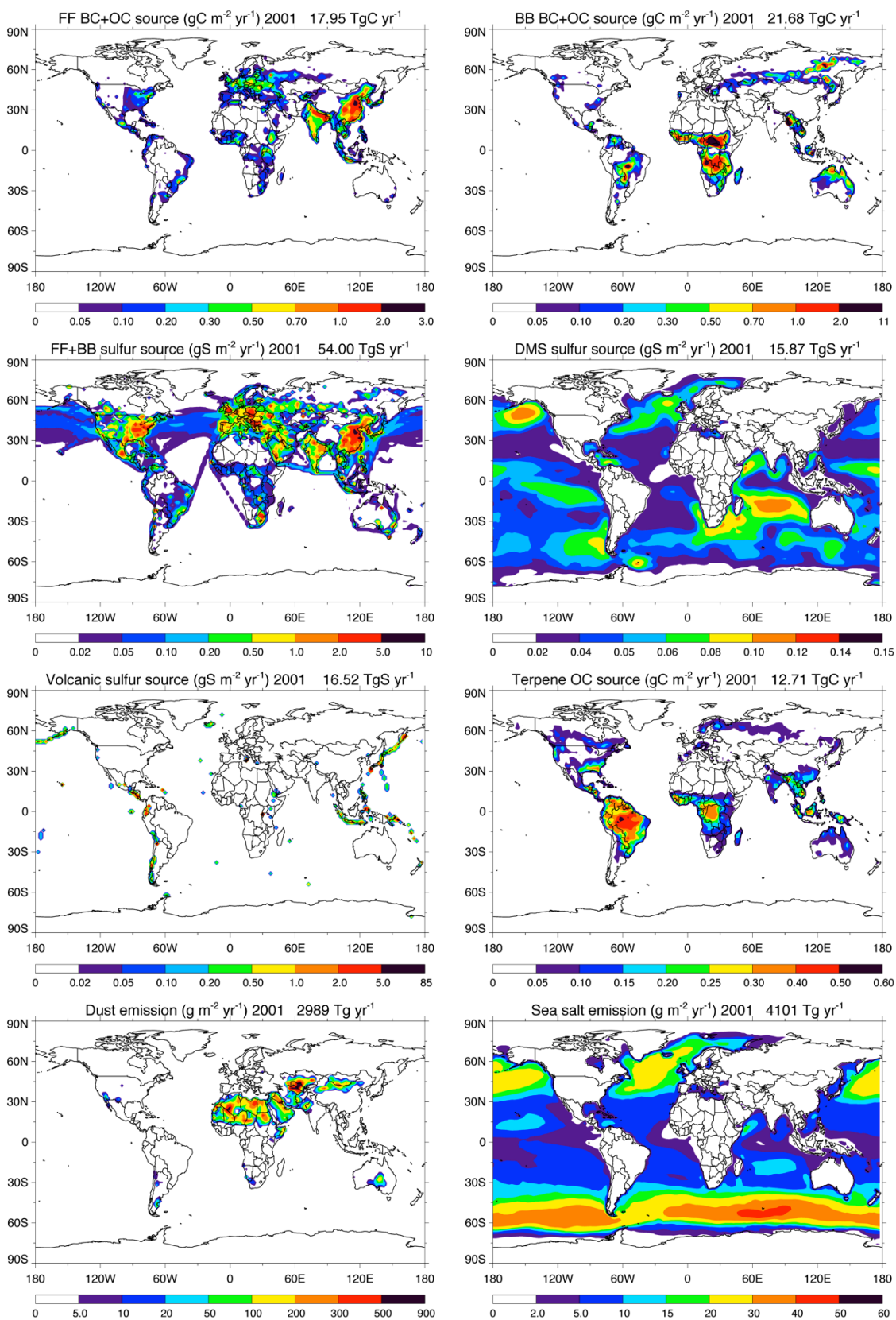


Fig. S1. Global sources of fossil fuel/biofuel (FF) OC+BC (top left), biomass burning (BB) OC+BC (top right), FF+BB SO_2 +sulfate (2nd row left), DMS (2nd row right), volcanic SO_2 (3rd row left), biogenic OC (3rd row right), dust (bottom left), and sea salt (bottom right) in 2001. The latter five are considered as natural sources.

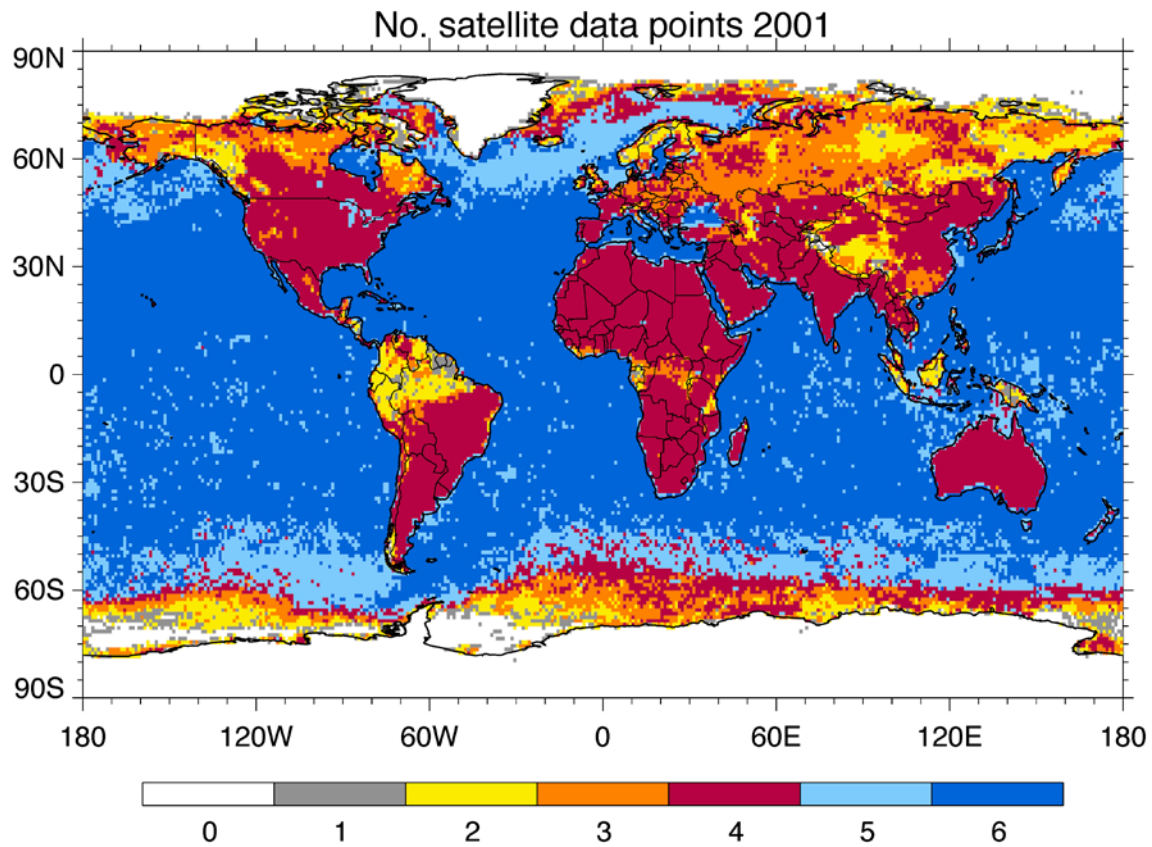


Fig. S2. Number of satellite data points of annual average AOD in 2001 for deriving the “data diversity” shown in Fig. 5 in the main section.

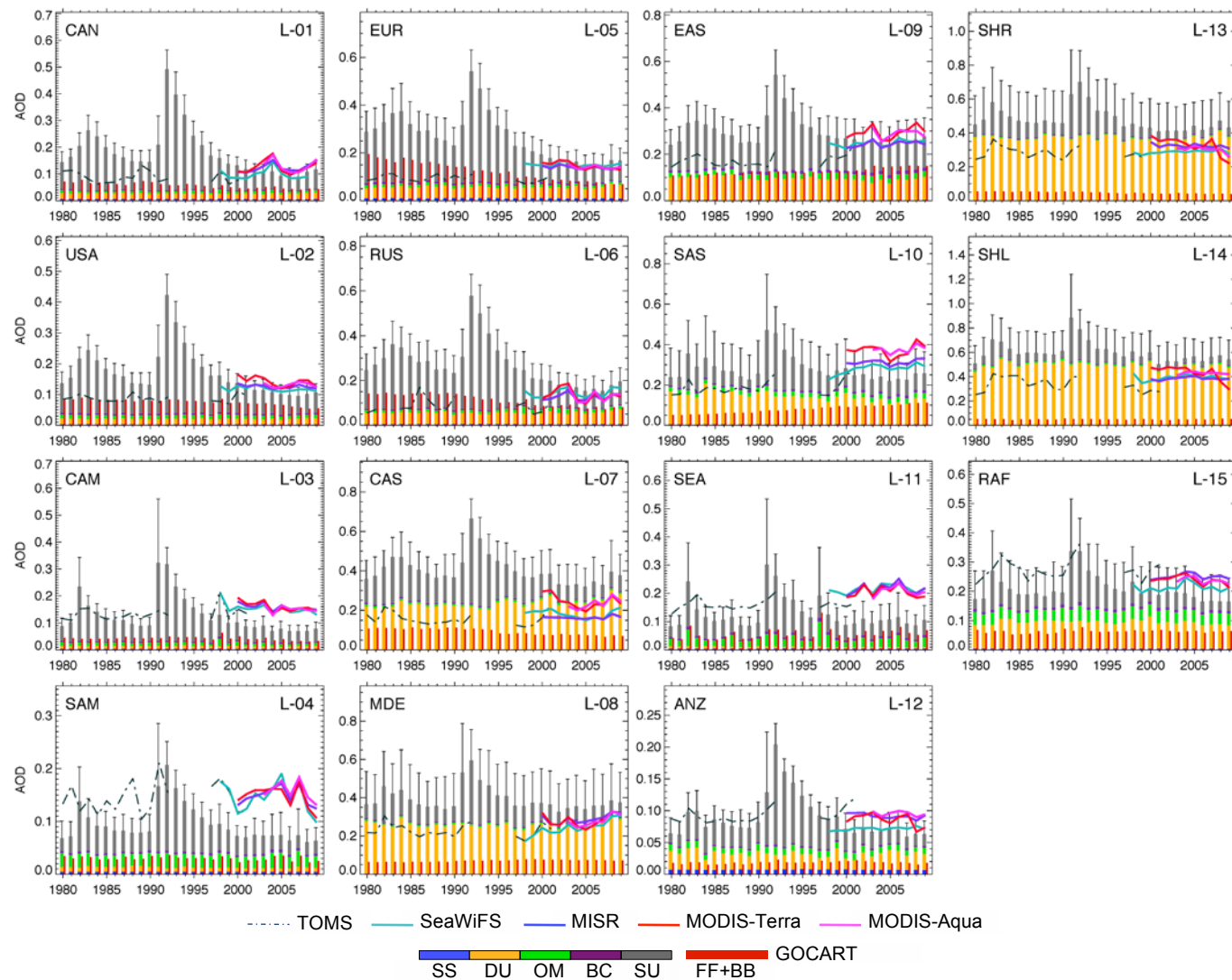


Fig. S3a. Regional annual average AOD from 1980 to 2009 for all 15 land regions. Region domains are shown in Fig. 1 and names listed in Table 1 in the main section. Legends are the same as Fig. 6a in the main section.

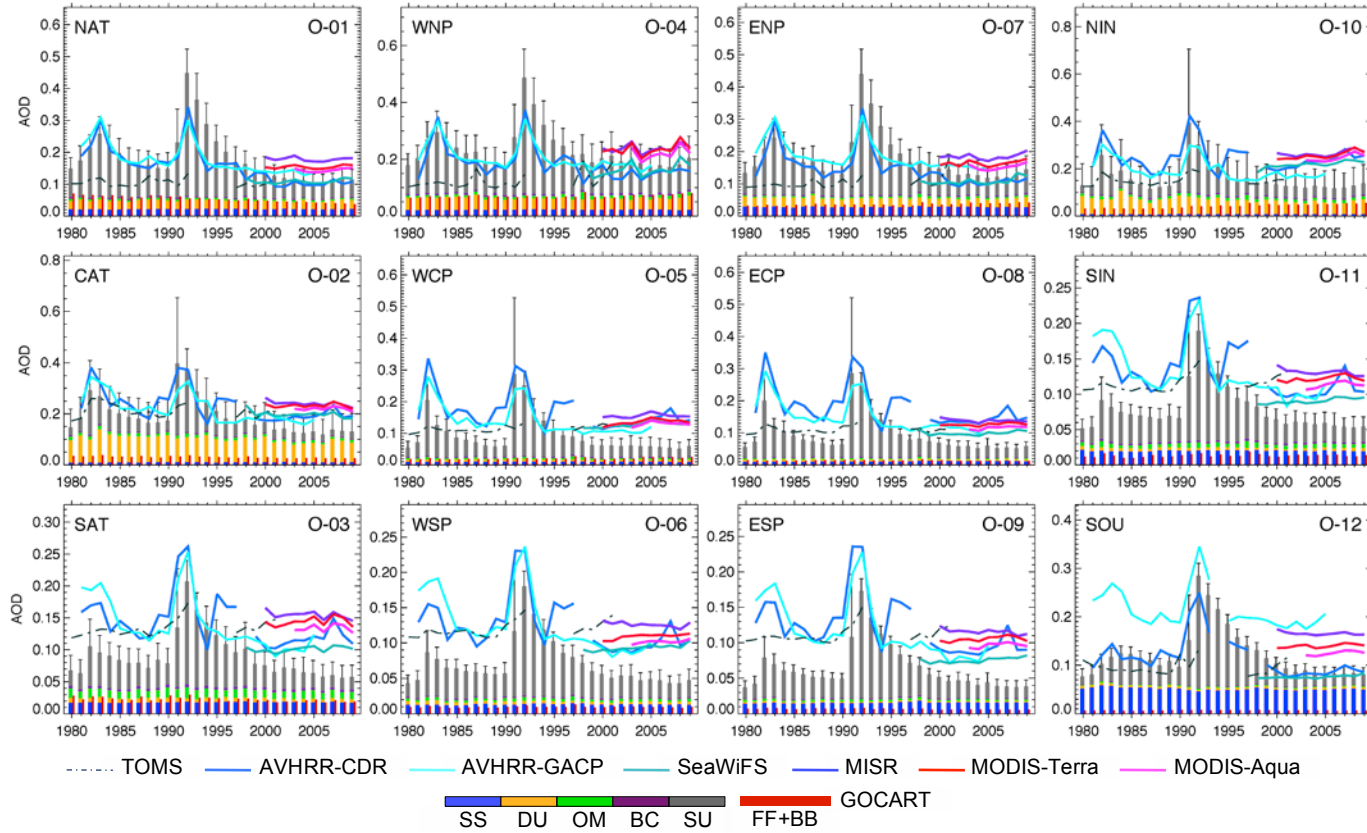


Fig. S3b. Regional annual average AOD from 1980 to 2009 for all 12 ocean regions. Region domains are shown in Fig. 1 and names listed in Table 1 in the main section. Legends are the same as Fig. 6b in the main section.

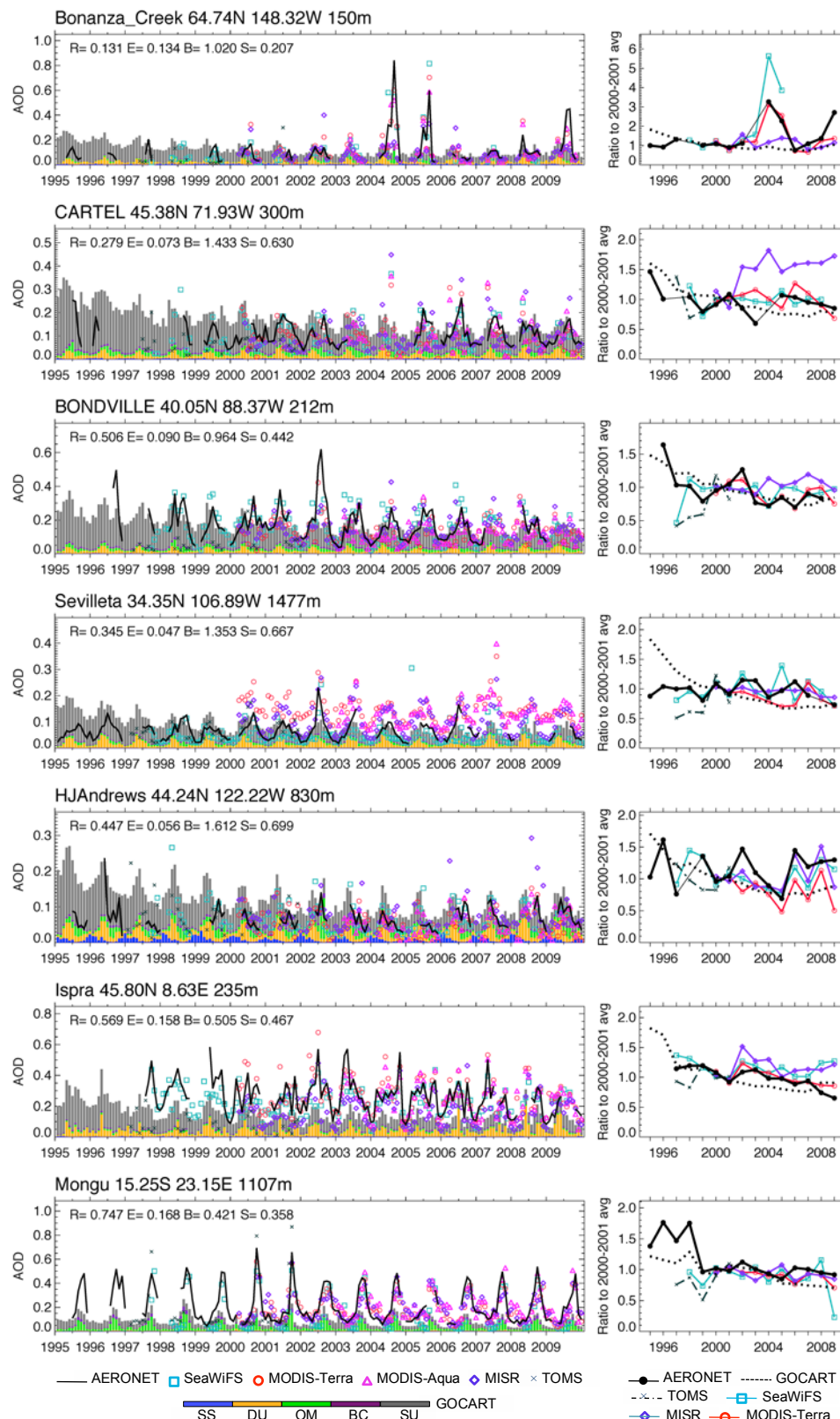


Fig. S4. Left column: Monthly AOD from AERONET and GOCART at seven sites that have data for at least 12 years but are not shown in Fig. 7 in the main text (site locations are shown in small circles in Fig. 3a). Right column: Ratio of annual mean AOD to the 2000-2001 average at corresponding sites. Legends are the same as Fig. 7. (Note: results over Mauna Loa are not shown because the AERONET sites is at 3.5 km but the model and satellite AOD contain significant amount PBL aerosols at their $2.5^{\circ} \times 2^{\circ}$ and $1^{\circ} \times 1^{\circ}$ spatial resolution, so the results are not comparable; and results over Wallops Island are also not shown because they are similar to GSFC for their close locations.)

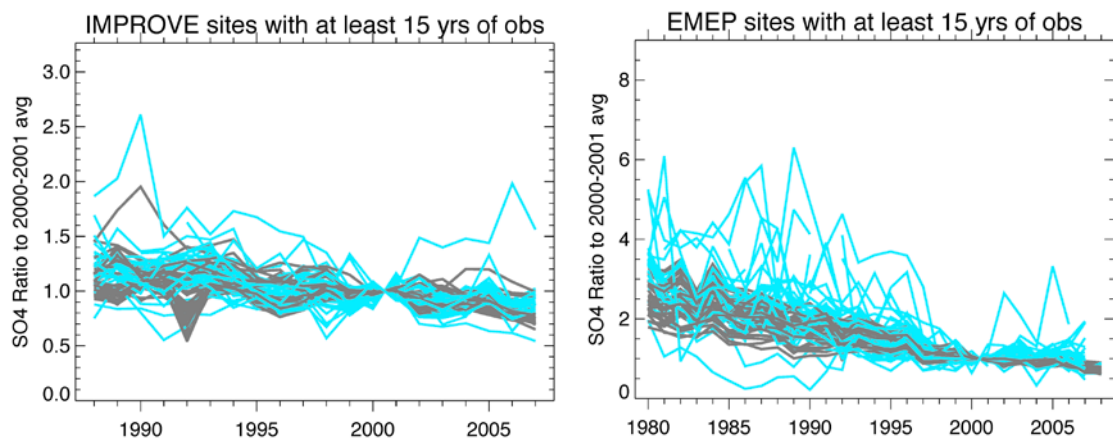


Fig. S5. Changes of surface concentration of sulfate expressed as the ratio of annual average to the 2000-2001 average for (left) IMPROVE and (right) EMEP measurements at sites with at least 15 years of data from the 1980s to 2000s. Data are shown in light blue and model results in dark grey.

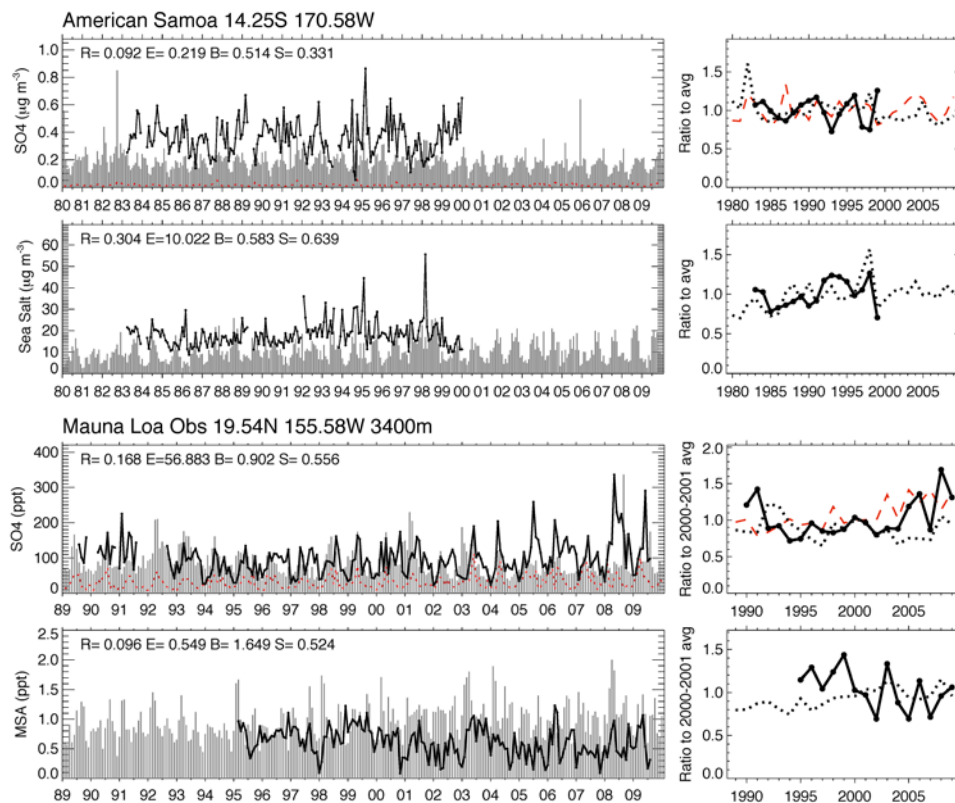


Fig. S6. Monthly surface concentrations (left column) and trends (right column) of sulfate and sea salt at American Samoa (top two panels) and sulfate and MSA at Mauna Loa Observatory. Data at American Samoa are from University of Miami, and that at Mauna Loa are from University of Hawaii. Site locations are in Fig. 3b (small red and orange circles, respectively, for Samoa and MLO). Legends are the same as Fig. 8.

